Anomalous size dependence of degenerate four-wave mixing due to double resonance of internal field and third-order susceptibility

Hajime Ishihara, Tomonari Amakata, and Kikuo Cho
Department of Physical Science, Graduate School of Engineering Science, Osaka University, Toyonaka, Osaka 560-8531, Japan
(Received 9 March 2001; revised manuscript received 17 August 2001; published 13 December 2001)

The degenerate four-wave mixing (DFWM) of weakly confined excitons in a mesoscopic thin film is studied by means of the nonlocal theory of nonlinear response, where the self-consistency between the induced polarization and the radiation field is considered. As a result, it is elucidated that the DFWM signal is greatly strengthened due to the double resonance of the internal field and the energy denominators of $\chi^{(3)}$, affecting both the incident and signal beams, and that the enhanced nonlinear response is originated from the transition associated with the nondipole type polarization pattern. The result clearly shows that the consideration of the nonlocal and self-consistent description of the response field is essential, which is in a striking contrast to the nonlinear response described in the long wavelength approximation.

DOI: 10.1103/PhysRevB.65.035305 PACS number(s): 78.66.−w, 42.65.−k, 78.20.Bh

I. INTRODUCTION

In the last decade, the size dependent nonlinear response of confined excitonic systems has been an interesting subject of study, and a lot of experimental and theoretical works have been made on this problem.[1–9] Nowadays, it is well recognized that the size dependent spectral structure of the nonlinear susceptibility is attributed to the size dependence of quantized excitonic levels and their oscillator strengths. In the strong confinement regime, for example, a shrinkage of the wave functions of electron-hole relative motion strengthens the oscillator strength,[10,11] which causes an enhancement of the nonlinear susceptibility. On the other hand, for the weak confinement regime, the size linear enhancement of the third-order susceptibility $\chi^{(3)}$ has been theoretically proposed,[1,2,5] where the oscillator strength increases linearly with the size as long as wave functions of center-of-mass (c.m.) motion of excitons are coherently extended to the whole volume of a sample, and this leads to the same behavior of $\chi^{(3)}$ per unit volume. As we see in these examples, most of considered mechanisms for the enhancement of nonlinear response are based on the size dependence of the oscillator strength. It is true that this picture is useful, to some extent, for the understanding of the size dependent nonlinear response. However, we should note that the concept of the oscillator strength is valid under the limited conditions. Namely, it can be used only when the long wavelength approximation (LWA) holds, and the LWA is no longer valid when the sample size approaches the wavelength of the light with relevant transition energy in the medium.[12] Such a wavelength can be much smaller than that in vacuum, and should be determined by the self-consistency conditions with the induced polarization and the electromagnetic field. In such a situation, the relationship between the induced polarization $\mathbf{P}(\mathbf{r})$ and internal field $\mathbf{E}(\mathbf{r})$ should be described in a nonlocal way. In the linear response, for example, it should be written as

$$\mathbf{P}(\mathbf{r}) = \int \chi(\mathbf{r},\mathbf{r}')\mathbf{E}(\mathbf{r}')d\mathbf{r}', \tag{1}$$

where χ is the linear susceptibility. It is recently elucidated that the nonlocality strongly affects the spatial structure of the resonant response field through the self-consistency between $\mathbf{E}(\mathbf{r})$ and $\mathbf{P}(\mathbf{r})$ even when the sample size is much smaller than the wavelength.[13] In other words, the internal field has nano-scale spatial structure reflecting that of the wavefunctions of the confined c.m. motion of excitons. Therefore, a more general treatment is necessary about the spatial and spectral structures of the internal field for the comprehensive understanding of the size dependent nonlinear response.

Noting the nonlocal nature, we have clarified that the resonant behavior of the internal field leads to a peculiar (resonant type) size enhancement of the pump-probe type nonlinear response.[14] This has demonstrated a new mechanism for the enhancement of nonlinear response. However, the pump-probe measurement is comparatively difficult for the experimental check of the proposed effect. Thus, it is desired to examine how the size dependent behavior of the internal field works in other types of resonant nonlinear processes. In this report, we deal with the degenerate four-wave-mixing (DFWM) process, which is one of the most popular and important nonlinear measurements, and in which a further enhancement effect turns out to be possible.

A key point in the present theory is the nonlocal and self-consistent description of the response field, which includes the size dependent radiative correction in the optical response and the nanoscale spatial variation of the internal field. Following the nonlocal nonlinear response theory[15,16] based on the perturbation expansion of density matrix, we incorporate the above effect in our calculations.

II. MODEL AND THEORY

Since we focus our interest on the weak confinement regime, we consider the c.m. motion of excitons explicitly, keeping the relative motion fixed. [The relative motion of

excitons is reflected in the parameter of bare exciton–radiation coupling (e.g., LT splitting).] Thus, we suppose a thin film consisting of N discrete layers that confines the component of the c.m. motion along the surface normal direction. The excitation on each layer is specified by the layer number j and the two-dimensional (2D) vector $\mathbf{k}$ in the lateral direction. If we restrict ourselves to the normal incidence, the contribution to the optical response arises only from the $\mathbf{k}=0$ one-exciton states, and the $\mathbf{K}=0$ two-exciton states consisting of $+\mathbf{k}_1$ and $-\mathbf{k}_1$ one-exciton states. In the following treatment, we consider only the contribution from $\mathbf{k}_1=0$ subspace as the two-exciton states. This assumption corresponds to the neglect of (i) the lateral transfer of excitons and (ii) the lateral interaction between two excitons.

The Hamiltonian of this model is

$$\mathcal{H}_0=\sum_{j=1}^{N}\varepsilon_0 a_j^\dagger a_j-b\sum_{j=1}^{N}(a_{j-1}^\dagger a_j+a_j^\dagger a_{j-1}) -\delta\sum_{j=1}^{N}a_j^\dagger a_{j+1}^\dagger a_j a_{j+1}, \tag{2}$$

where $a_j^\dagger$ and a_j are the creation and annihilation operators of an exciton on the jth site, ε_0 the excitation energy of each site, b the transfer energy, and we introduce the virtual sites $j=0$ and $N+1$ on which the amplitude of excitons is supposed to be zero. The lattice constant is taken to be the unit of length. The third term, exciton-exciton interaction, is introduced to allow biexciton states. Though this model of interaction is considerably simplified, some effects of biexcitons in DFWM can be examined qualitatively. As for one-exciton states, the eigenfunctions and eigenvalues can be written as

$$|K_n\rangle=\sqrt{\frac{2}{N+1}}\sum_j \sin(K_n j)a_j^\dagger|0\rangle \tag{3}$$

and

$$E_1(n)=\varepsilon_0-2b\cos K_n, \tag{4}$$

respectively, where the allowed values of K_n are

$$K_n=\frac{n\pi}{N+1},\quad \{n=1,2,\ldots,N\}. \tag{5}$$

As for the two-exciton states, we expand them as

$$|\mu\rangle=\sum_{i<j}C_{i,j}^{(\mu)}a_j^\dagger a_i^\dagger|0\rangle, \tag{6}$$

and calculate their eigenvalues $\{E_\mu\}$ and the coefficients $\{C_{i,j}^{(\mu)}\}$ numerically, where we consider the Pauli exclusion principle that prohibits double excitations on one site. The Pauli effect and the third term of right-hand side of Eq. (2) are the sources of nonlinearity of this model.

When we limit ourselves to the normal incidence, and when the excitonic Bohr radius is very small like that of CuCl, we can very well reproduce the linear optical spectra even for the Wannier excitonic systems by this model choosing an appropriate parameter value of the LT splitting.[18] Furthermore, the simplicity of this model enables us to explicitly treat the whole functional space up to the two-exciton states, which is enough for the evaluation of the nonlinearity arising from the state-filling and the biexciton effect.[19] On the other hand, neglecting the lateral energy transfer may change the absolute value of $\chi^{(3)}$ near one-exciton resonance from that of three dimensional materials because the enhancement effect of $\chi^{(3)}$ due to the finite transfer[20] is changed. (How $\chi^{(3)}$ changes with the value of the transfer energy is discussed in detail in Ref. 20.) And also the contribution from the induced absorption by two-exciton states becomes particular one reflecting the one-dimensional nature. However, these changes of the quantitative value of nonlinear signals never spoil our discussion on the essential trend of the size dependence ruled by the resonant enhancement of the internal field.

Supposing the normal incidence of the pump and probe beams, we calculate the self-consistent internal fields for them with the standard expression of the exciton-radiation interaction Hamiltonian

$$\mathcal{H}'=-\sum_l\sum_p \hat{P}_l\mathcal{E}_l(p)\exp(-i\omega_p t), \tag{7}$$

where $\mathcal{E}_l(p)$ is the amplitude of internal field on the lth site with the frequency ω_p, $\hat{P}_l$ is the polarization operator on the same site, namely,

$$\hat{P}_l=Ma_l+M^*a_l^\dagger, \tag{8}$$

and M is the transition dipole matrix per site. We assume the pump intensity is limited within the $\chi^{(3)}$ regime and the probe beam is much weaker than that. Under this condition, the third order polarization can be described, as a good approximation, in terms of the amplitudes of these beams calculated within the linear response. Thus, we solve the Maxwell's equation including the linear nonlocal polarization whose explicit form is

$$P_j^{(1)}(\omega_p)=\frac{M^2}{v_0}\left(\frac{2}{N+1}\right)^{1/2}\sum_n\frac{\sin(K_n j)F_n^{(p)}}{E_1(n)-\omega_s-i\Gamma}e^{-i\omega_p t}, \tag{9}$$

where $p=1$ and 2 representing the probe and pump beam frequencies, respectively, v_0 is the unit cell volume. The definition of $F_n^{(p)}$ is

$$F_n^{(p)}=\left(\frac{2}{N+1}\right)^{1/2}\sum_j \sin(K_n j)\mathcal{E}_j(p), \tag{10}$$

and Γ is the phenomenologically introduced constant for the transverse damping. We can rewrite the Maxwell equations to the linear simultaneous equations for $\{F_n\}$,[15] which can be analytically solved for the present model. The explicit expressions of the Maxwell's equations and their solutions are given in the Appendix.

In terms of the internal amplitudes of the pump and probe beam, the third order nonlinear polarization with the frequency $\omega_s(=2\omega_2-\omega_1)$ is written as

$$\begin{aligned}P_j^{(3)}(\omega_s)=\frac{M^4}{v_0}\left(\frac{2}{N+1}\right)^{1/2}\sum_n \sin K_n j \\ \times\Bigg[\sum_m A(K_n,K_m;\omega_1,\omega_2)F_n^{(2)}F_m^{(2)}F_m^{(1)*} \\ +\sum_m\sum_{n',m'} B(K_n,K_m,K_{n'},K_{m'};\omega_1,\omega_2) \\ \times F_{n'}^{(2)}F_{m'}^{(2)}F_m^{(1)*}\Bigg]\exp(-i\omega_s t),\end{aligned} \tag{11}$$

where we pick up the contributions of the most (triply) resonant terms. The explicit expressions of A and B in Eq. (11) are

$$\begin{aligned}A(K_n,K_m;\omega_1,\omega_2)=\frac{1}{(E_1(n)-(2\omega_2-\omega_1)-i\Gamma)(\omega_2-\omega_1+i\gamma)}\left[\frac{1}{E_1(m)-\omega_1+i\Gamma}-\frac{1}{E_1(m)-\omega_2-i\Gamma}\right] \\ +\frac{1}{(E_1(n)-(2\omega_2-\omega_1)-i\Gamma)(E_{nm}-(\omega_2-\omega_1)-i\Gamma_{nm})}\left[\frac{1}{E_1(n)-\omega_2-i\Gamma}-\frac{1}{E_1(m)-\omega_1+i\Gamma}\right]\end{aligned} \tag{12}$$

and

$$\begin{aligned}B(K_n,K_m,K_{n'},K_{m'};\omega_1,\omega_2)=\sum_\mu 4\bar{C}_{n'm'}^{(\mu)}\bar{C}_{nm}^{(\mu)}\Bigg[\frac{1}{E_{\mu m}-(2\omega_2-\omega_1)-i\Gamma}\Bigg\{\frac{1}{E_{mm'}+(\omega_2-\omega_1)+i\Gamma_{mm'}} \\ \times\left(\frac{1}{E_1(m')-\omega_2-i\Gamma}-\frac{1}{E_1(m)-\omega_1+i\Gamma}\right)-\frac{1}{(E_\mu-2\omega_2-2i\Gamma)(E_1(m')-\omega_2-i\Gamma)}\Bigg\} \\ +\frac{1}{(E_1(n)-(2\omega_2-\omega_1)-i\Gamma)(E_\mu-2\omega_2-2i\Gamma)(E_1(n')-\omega_2-i\Gamma)}\Bigg],\end{aligned} \tag{13}$$

respectively, where

$$E_{\mu n}=E_\mu-E_1(n), \tag{14}$$

$$E_{nm}=E_1(n)-E_1(m), \tag{15}$$

$$\Gamma_{nm}=\gamma(n=m), \tag{16}$$

$$=\Gamma(n\neq m), \tag{17}$$

and

$$\bar{C}_{n,m}^{(\mu)}=\frac{1}{N+1}\sum_{l'<l} C_{l,l'}^{(\mu)}(\sin K_n l\sin K_m l'+\sin K_n l'\sin K_m l). \tag{18}$$

In this calculation, we introduce the phenomenological longitudinal damping constant γ, in addition to Γ. However, the nonlinear damping effects such as the excitation-induced dephasing[17] are excluded because they do not have a qualitatively essential role in our considered mechanism for the weak excitation limit. The Maxwell's equation including the nonlinear polarization (11) and the linear polarization for the signal frequency can also be rewritten into the linear equation for $\{F_n^{(p)}\}$ if $\{F_n^{(2)}\}$ and $\{F_n^{(1)}\}$ are treated as given values. We solve this equation, and then obtain the signal field outside the film by using the Maxwell's boundary conditions. The details of these calculations are also given in the Appendix.

III. RESULTS

The following numerical calculations are performed for the Z_3 exciton of CuCl that is a typical single component exciton. The present model is well applicable to this system

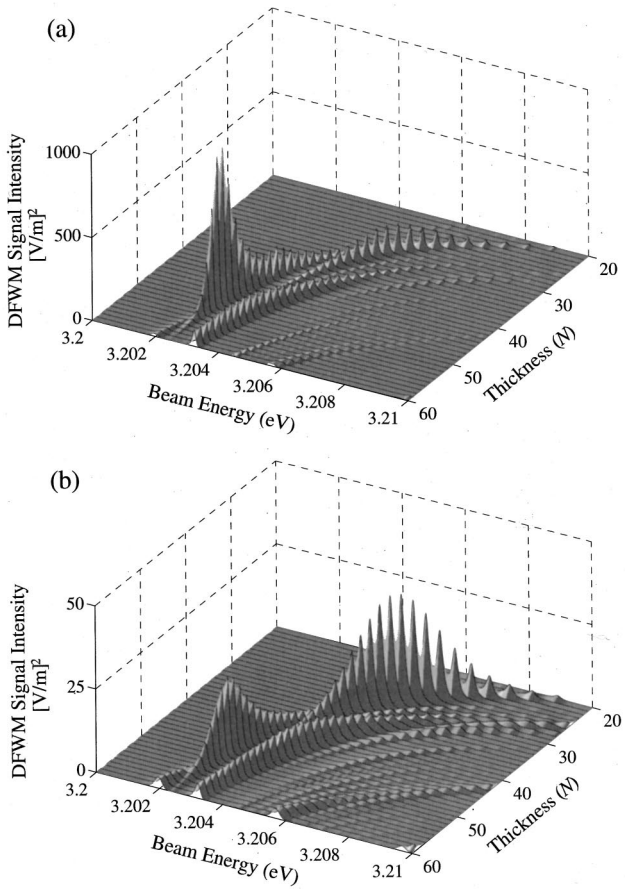

FIG. 1. Intensity of the DFWM signal as a function of beam energy and thickness (N). The lattice constant is 0.54 nm. The amplitudes of the pump and probe beams are 2.4×10^5 V/m and 1.2×10^3 V/m. (a) Γ (γ) = 0.06 (0.02) meV. (b) Γ (γ) = 0.12 (0.04) meV.

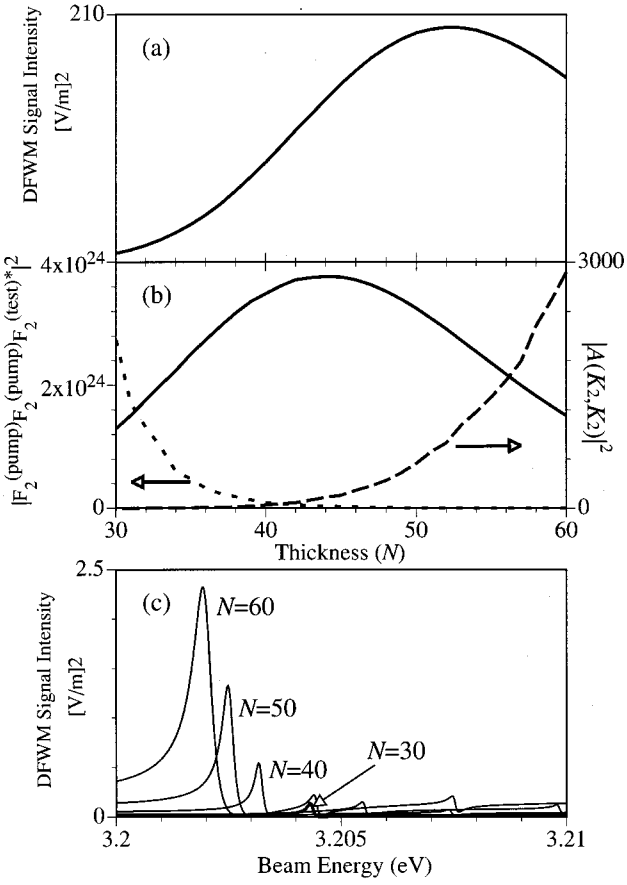

FIG. 2. (a) Peak value of the DFWM signal intensity vs N. The term including $A(K_2,K_2;\omega,\omega)$ alone is considered. (b) The peak values of $|F_2^{(2)}F_2^{(2)}F_2^{(1)}A(K_2,K_2;\omega,\omega)|^2$ (solid line), $|F_2^{(2)}F_2^{(2)}F_2^{(1)}|^2$ (broken line), and $|A(K_2,K_2;\Omega_2,\Omega_2)|^2$ (dotted line). The unit of the first quantity is arbitrary. The second quantity is normalized by (pump intensity)$^2\times$ (probe intensity). The third one is in unit of $|M|^4/v_0$. (c) The DWFM spectra for the several values of N. The value of $F_2^{(2)}F_2^{(2)}F_2^{(1)}A(K_2,K_2;\omega,\omega)$ is taken to be constant in this calculation.

because the Bohr radius of Z_3 exciton is considerably small (about 0.6 nm). We use the following parameters representative of CuCl: $\omega_T=3202.2$ meV, $b=57.0$ meV, $4\pi|M|^2/v_0=5.7$ meV, $\varepsilon_b=5.6$, and $\bar{\delta}=195$ meV, where ω_T is the energy of the bottom of exciton band for $N\to\infty$, namely, $\omega_T=\varepsilon_0-2b$.

A. DFWM spectra

Figure 1 shows the DFWM signal intensity as a function of the beam energy and N for the two different damping values. (The smaller value of Γ is chosen from the fitting parameter in Ref. 21.) In both cases, there are several peak structures due to the excitonic transitions. Among these structures, we should note a particular one around the lowest one-exciton resonance that is strongly enhanced at a particular size in the case of the smaller damping [Fig. 1(a)]. For the larger damping [Fig. 1(b)], such an enhancement cannot be seen. These peak structures are attributed to the transitions between the ground and one-exciton states and between the one- and two-exciton states, whose resonance poles are included in the nonlinear susceptibility. The former poles are included in A and B, and the latter are included only in B, in the square bracket in Eq. (11). The cause of the large DFWM signal at a particular size is the size-resonant enhancement of the internal field with a nondipole type spatial pattern as we will discuss below.

B. Analysis of spectra

Evaluating individual terms in Eq. (11), we find that one of main contributions in the enhanced signal comes from the term including $A(K_2,K_2;\omega_1,\omega_2)$ whose explicit expression for $\omega_2=\omega_1=\omega$ is

$$A(K_2,K_2;\omega,\omega)=-\frac{4\Gamma}{\gamma}\frac{1}{\{E_1(2)-\omega-i\Gamma\}[\{E_1(2)-\omega\}^2+\Gamma^2]}. \tag{19}$$

In Fig. 2(a), we show the size dependence of the peak value in DFWM spectrum in case that we consider the contribution

from this term alone. The cause of the large contribution of this term is the enhancement of F_2 component in the internal field. (Note that $\{F\}$ are nothing but the components of the internal field when we expand it with the bases of quantized one-exciton states.) This component is associated with the second one-exciton state $|K_2\rangle$, and is enhanced at its resonance energy (Ω_2) including the radiative shift. The peak value of $|F_2|^2$ increases with the size, which is favorable for the size enhancement of the DFWM signal. On the other hand, the radiative shift also increases with the size, which decreases the value of $\chi^{(3)}$ at Ω_2 due to off resonance. As a consequence of the balance of these two effects, the spectral peak of the DFWM signal has a maximum value at a particular size. This situation is explained in Fig. 2(b), where we show the size dependence of the peak values of $|F_2^{(2)}F_2^{(2)}F_2^{(1)}|^2$ (internal field) and $|A(K_2,K_2;\Omega_2,\Omega_2)|^2$, and a product of them. In this figure, the first (second) quantity increases (decreases) with the size, and their product has a maximum value at a certain size.

The enhancement of $|F_2|^2$ can also be understood as a result of nanoscale Fabry-Pérot interference of excitonic polaritons.[13] Since this interference becomes dim if the excitonic coherence is not sufficient, the remarkable enhancement of DFWM signal does not appear when the damping constant is large [Fig. 1(b)].

The noteworthy point in the above effect is that the main contribution to the signal enhancement comes from the nondipole type transition. (Note that the wave function of $|K_2\rangle$ state has a node in the surface normal direction.) This means that the self-consistent field has no longer the long-wavelength when the size is approaching $N=50$ and exhibits a large spatial distribution. In contrast to the large contribution of F_2 component, F_1 (dipole type) component is very small around the lowest one-exciton state ($|K_1\rangle$) because of its large radiative shift. (For the film geometry, the radiative shift of the lowest one-exciton state is generally positive and larger than that of the second one.[22]) Namely, the large coupling between the radiation field and $|K_1\rangle$ state suppresses the amplitude of F_1 component around bare $|K_1\rangle$ level, which leads to its very small contribution to the DFWM signal.

Another important factor in this large nonlinear response is the enhancement of the internal field of nonlinear signal itself. To show this effect, we calculate the same quantity as in Fig. 2(a) without the effect of resonance in A and the size dependence of the incident fields. Namely, we take $A(K_2,K_2;\omega,\omega)F_2^{(2)}F_2^{(2)}F_2^{(1)}$ as a constant value. However, the DFWM signal still has size dependence [Fig. 2(c)]. This indicates that the internal field of DFWM signal is also enhanced in the film due to the nanoscale Fabry-Pérot interference. This multiple enhancement of the internal field makes the DFWM signal much more prominent than that in the pump-probe spectroscopy[14].

The contributions from the second term in the square bracket in Eq. (11) are mainly attributed to the transitions between [one-exciton state]-[two-exciton state]. The dominant contribution is from the term including B in Eq. (11) that contains the factor

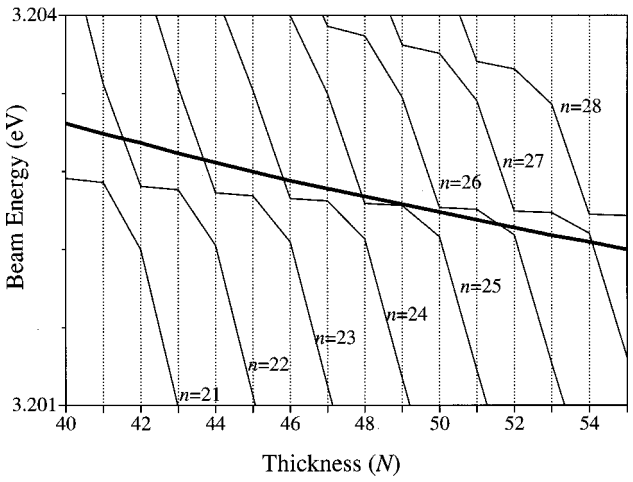

FIG. 3. The size dependence of the transition energy between the second one-exciton state and nth two-exciton state. The thick solid line shows the energy where $|F_2|^2$ takes a maximum value.

$$\frac{1}{(E_{\mu 2}-\omega-i\Gamma)\{[E_1(2)-\omega]^2+\Gamma^2\}}. \tag{20}$$

For the DFWM process, the contributions from the deeply bound two-exciton states (e.g., excitonic molecules in CuCl) are very small because of the large off-resonance. On the other hand, the contributions of the scattering two-exciton states appears remarkably, which is resonantly strengthened when the [one-exciton]-[two-exciton] transition energy coincides with the energy for the resonant enhancement of a particular component of the internal field (F_2 component in the present case). Figure 3 shows such a condition is realized near $N=50$ for the present model. The latter contributions either enlarge or reduce the signal intensity shown in Fig. 2(a) according to the relative phase between the first and second terms in the square bracket in Eq. (11).

IV. DISCUSSIONS

In condensed matter, an excitation energy given to a particular site (atom or molecule) generally propagates to the other sites through an electronic intersite interaction, which means the wave functions of excited states are coherently extended. Since this effect is the origin of nonlocality, the nonlocal response is general for the solids. The nonlocal effect is highly important especially in the ''weak confinement regime'' where the c.m. motion of excitons is confined. In this regime, each quantized level exhibits a particular spatial pattern according to the boundary conditions of the system. The induced polarizations reflect these patterns of the resonant levels due to the transfer effect even if the radiation field of the incident light has long wavelength without any structure in the medium. Since such polarizations radiate light again and it contributes to the response field, the self-consistent internal field (Maxwell's field) also has nanoscale spatial structure similar to those of the induced polarizations. Thus, in the nonlocal media, the radiation-matter coupling is dominated by the spatial structures of the matter excited states, where the electronic intersite interaction plays an es-

sential role. It is interesting to compare this situation with that of the recently discussed regular array of semiconductor quantum well's (RAQW's) (Refs. 23,24) by which one can control the radiation-matter coupling through the interwell distance and the number of wells. In the RAQW's, individual wells are so thin that they can be described in LWA, and they couple with each other only via radiation because the interwell distance is comparable to the light wavelength. Thus, in this system, electronic interwell interaction does not play an important role in principle, while the arrangement structure of the quantum wells dominates the radiation-matter coupling. For example, one can realize the Bragg or anti-Bragg condition controlling the interwell coupling via radiation field.

In the previous sections, we clearly show that an ''unusual situation'' arises if the spatial extension of the matter excited state is comparable with or larger than the wavelength of the resonant light in the medium, namely, the higher multipole transition makes a large contribution to some nonlinear processes. As we see in the previous section, the main contribution to the enhanced DFWM signal does not come from an electric dipole transition, but from a quadrupole-type transition, where the induced polarization of the relevant transition is polarized laterally and has a node in the surface normal direction. Generally, the radiative shift of the higher excitonic level with a nondipole type spatial structure is smaller than that of the lowest one. This situation leads to a double resonance of the internal field and the third-order susceptibility because the response field becomes strong very near the matter (bare excitonic) level in some condition. For the response of the lowest level, on the other hand, the internal field near the bare excitonic level is usually much suppressed because of the large ladiative shift. This is why the contribution from $|K_2\rangle$ state is much larger than that from $|K_1\rangle$ state in the present case. Since the condition of the double resonance heavily depends on the system size, the size dependence of the nonlinear response can be quite different from that proposed in the former works based on the $\chi^{(3)}$ discussion alone.[1,2,5] Especially in the DFWM process, we wish to emphasize the fact that the enhancement of the internal field occurs not only on the incident (pump and probe) beams but also on the signal beam itself, which makes the enhancement of the DFWM signal much more remarkable than that in the pump-probe spectroscopy.[14] This effect has a good analogy with the mechanism of the surface enhanced Raman scattering where the double enhancement of both the incident and scattered lights plays an important role to enhance the signal intensity.[25]

Since the calculations in this paper are performed on a particular one-dimensional model, the quantitative results may be peculiar to this model. However, the essential mechanism of the above enhancement should be general for the nonlocal systems, and the similar effect is expected to appear in any kinds of materials to a greater or less extent. Actually, the recent experimental results for the GaAs thin films in the weak confinement regime[26] and the analysis for them[27] clearly shows that our proposed effect works if the sample has good quality. Though the present model can not be simply applied to GaAs for the quantitative discussion, the study with the more general and realistic model would reveal the similar mechanism for this material.

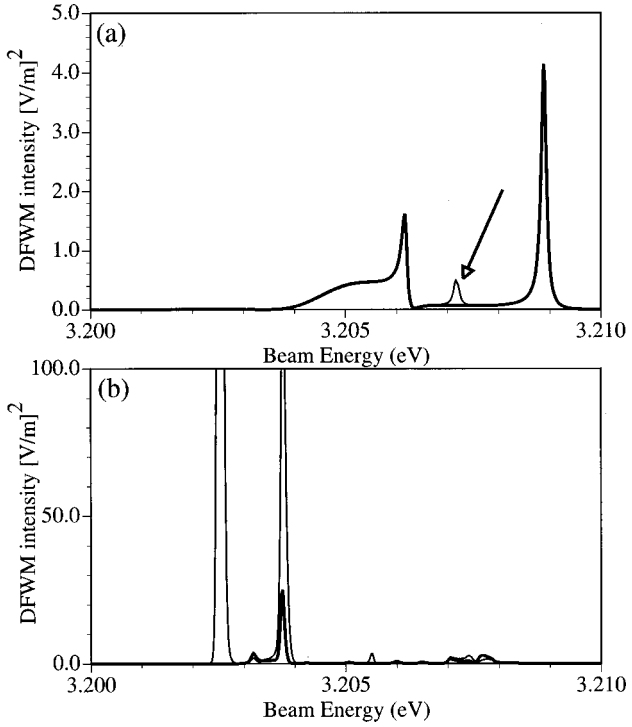

FIG. 4. The comparison between the DFWM spectra calculated with the nonlocal (thin line) and LWA method (thick line). (a) $N=20$, (b) $N=50$.

Finally, we add the results of comparison between the nonlocal and the LWA calculation to see how the nonlocal effect is essential to enhance the DFWM signal. Since we concentrate on the nonlinear part in this comparison, we treat the linear polarization in nonlocal way, and the third order polarization is treated either nonlocally or in the LWA. (The study of nonlocal vs LWA for the linear response has already been given in Ref. 13.) In the LWA treatment, we neglect the site dependence of the pump and probe field in $P^{(3)}$ as

$$F_n{}^{(s)}=\left(\frac{2}{N+1}\right)^{1/2}\sum_j \sin(K_n j)\mathcal{E}_j(s)\rightarrow\mathcal{E}(s) \times\left(\frac{2}{N+1}\right)^{1/2}\sum_l \sin(Kl), \tag{21}$$

and attribute $\mathcal{E}(s)$ to the amplitude averaged over the sites. The comparison for the thinner case ($N=20$) is shown in Fig. 4(a). Although two results are almost the same, a small difference is found near the second one-exciton resonance [indicated with an arrow in Fig. 4(a)], namely, a small peak structure appears in the nonlocal calculation, whereas no structure is found for the LWA calculation. This peak is due to the F_2 component of the internal field. For small N, the contribution from this component is not conspicuous. For the thicker case ($N=50$), on the other hand, this component is enhanced and greatly strengthens the DFWM signal, which leads to a significant difference between the spectrum by nonlocal method and that by LWA method [Fig. 4(b)]. This

demonstration clearly indicates that the nanoscale spatial structure of the internal field is essential for the enhancement of the nonlinear signal.

Although we focus our attention on the enhancement effect of DFWM in this paper, the nonlocality affects any aspect of the optical response in principle. For example, the spatial structure of the c.m. wave function of excitons also causes a peculiar size dependence of the radiative width. If the sample size approaches the wavelength of resonant light which is determined by the background dielectric constant alone, the radiative coupling of the relevant state should be described with the proper consideration of the spatial structures of both the excitons and radiation. Recently, the very fast radiative decay of the $|K_2\rangle$ state has been observed for a 110-nm-thick GaAs film,[28] which is beyond the effect due to so-called size-linear enhancement of the oscillator strength[2] based on LWA. We are now studying this novel type of radiative decay by means of the nonlocal theory and will discuss it in detail in the next publication.

ACKNOWLEDGMENTS

The authors are grateful to Dr. Isu and Mr. Akiyama for useful discussions on their experimental results before publication. Numerical calculations were performed in part on FACOM VPP500 in Supercomputer Center, Institute for Solid State Physics, University of Tokyo. This work was supported in part by Grants-in-Aid for COE Research (Grant No. 10CE2004) of the Ministry of Education, Science, Sports and Culture of Japan.

APPENDIX: MAXWELL'S EQUATION AND BOUNDARY CONDITIONS

1. For linear response

The linear Maxwell's equation (for the discrete lattice model) including $P_j^{(1)}(\omega_p)$ is

$$\begin{aligned}[\Delta^2-(2\cos q_p-2)]\mathcal{E}_j(\omega_p)&=-Q_p^2P_j^{(1)}(\omega_p)\\&=-B_p^{(1)}\left(\frac{2}{N+1}\right)^{1/2}\sum_n \sin K_n j\frac{F_n^{(p)}}{E_1(n)-\omega_p-i\Gamma},\end{aligned} \tag{A1}$$

where

$$\Delta^2\mathcal{E}_j=\mathcal{E}_{j+1}-2\mathcal{E}_j+\mathcal{E}_{j-1}, \tag{A2}$$

$$q_p=a_0\frac{\omega_p}{c}\sqrt{\varepsilon_b}, \tag{A3}$$

$$B_p^{(1)}=Q_p^2\frac{M^2}{v_0}, \tag{A4}$$

$$Q_p^2=a_0^2\frac{4\pi\omega_p^2}{c^2}, \tag{A5}$$

and $p=1,2$ represent for the probe and pump frequencies, respectively, j the site index, a_0 the lattice constant, c the light velocity, and ε_b the background dielectric constant. The formal solution of Eq. (A1) can be written as

$$\mathcal{E}_j(\omega_p)=\mathcal{E}e^{iq_pj}+\overline{\mathcal{E}}e^{iq_p(N+1-j)}-\sum_n\frac{\sin K_n j}{2\cos K_n-2\cos q_p}\tilde{A}(K_n), \tag{A6}$$

where

$$\tilde{A}(K_n)=B_p^{(1)}\left(\frac{2}{N+1}\right)^{1/2}\frac{F_n^{(p)}}{E_1(n)-\omega_p-i\Gamma}. \tag{A7}$$

With Eq. (A6) and the definition (10), we can obtain the equation to determine $\{F_n^{(p)}\}$ as

$$\begin{aligned}\left(\frac{N+1}{2}\right)^{1/2}&\left[1+\frac{B_p^{(1)}}{2\cos K_n-2\cos q_p}\frac{1}{E_1(n)-\omega_p-i\Gamma}\right]F_n^{(p)}\\&=\mathcal{E}\frac{\sin K_n}{2\cos K_n-2\cos q_p}[(-1)^ne^{iq_p(N+1)}-1]\\&\quad+\overline{\mathcal{E}}\frac{\sin K_n}{2\cos K_n-2\cos q_p}[(-1)^n-e^{iq_p(N+1)}].\end{aligned} \tag{A8}$$

If we write incident, reflected and transmitted fields as

$$\mathcal{E}_ie^{ik_0j}, \tag{A9}$$

$$\mathcal{E}_re^{-ik_0j}, \tag{A10}$$

and

$$\mathcal{E}_te^{ik_0(j-N-1)}, \tag{A11}$$

respectively, we obtain the Maxwell's boundary conditions at the front surface, as

$$\mathcal{E}_i+\mathcal{E}_r=\mathcal{E}+\overline{\mathcal{E}}e^{iq_p(N+1)} \tag{A12}$$

$$\begin{aligned}\mathcal{E}_i(e^{ik_0}-1)+\mathcal{E}_r(e^{-ik_0}-1)&=\mathcal{E}(e^{iq_p}-1)+\overline{\mathcal{E}}(e^{-iq_p}-1)e^{iq_p(N+1)}\\&\quad-\sum_n\frac{\sin K_n}{2\cos K_n-2\cos q_p}\tilde{A}(K_n),\end{aligned} \tag{A13}$$

and at the back surface, as

$$\mathcal{E}e^{iq_p(N+1)}+\overline{\mathcal{E}}=\mathcal{E}_t \tag{A14}$$

$$\mathcal{E}(1-e^{-iq_p})e^{iq_p(N+1)}+\overline{\mathcal{E}}(1-e^{iq_p})-\sum_n\frac{(-1)^n\sin K_n}{2\cos K_n-2\cos q_p}\tilde{A}(K_n)=\mathcal{E}_t(1-e^{-ik_0}). \tag{A15}$$

With the given incident amplitude $\mathcal{E}_i$, all the amplitudes $\mathcal{E},\overline{\mathcal{E}},\mathcal{E}_r,\mathcal{E}_t$ and $\{F_n^{(s)}\}$ can be determined by using the simultaneous equations (A8),(A12),(A13),(A14),(A15).

2. For the third order nonlinear response

The third order nonlinear Maxwell's equation (for the discrete lattice model) is

$$
\begin{aligned}
&[\Delta^2-(2\cos q_s-2)]\mathcal{E}_j(\omega_s)\\
&\quad=-Q_3^2[P_j^{(1)}(\omega_3)+P_j^{(3)}(\omega_s)]\\
&\quad=-\left(\frac{2}{N+1}\right)^{1/2}\Bigg[B_3^{(1)}\sum_n \sin K_n j\frac{F_n^{(3)}}{E_1(n)-\omega_s-i\Gamma}+B_3^{(3)}\\
&\qquad\times\sum_n \sin K_n j\Bigg\{\sum_m A(K_n,K_m;\omega_1,\omega_2)F_n^{(2)}F_m^{(2)}F_m^{(1)*}\\
&\qquad+\sum_m\sum_{n',m'} B(K_n,K_m,K_{n'},K_{m'};\omega_1,\omega_2)\\
&\qquad\times F_{n'}^{(2)}F_{m'}^{(2)}F_m^{(1)*}\Bigg\}\Bigg],
\end{aligned}
\tag{A16}
$$

where

$$
q_s=a_0\frac{\omega_s}{c}\sqrt{\varepsilon_b},
\tag{A17}
$$

$$
B_s^{(1)}=Q_s^2\frac{M^2}{v_0},
\tag{A18}
$$

$$
B_s^{(3)}=Q_s^2\frac{M^4}{v_0},
\tag{A19}
$$

$$
Q_s^2=a_0^2\frac{4\pi\omega_s^2}{c^2},
\tag{A20}
$$

and ω_s means signal frequency. We substitute $\{F_n^{(1)}\}$ and $\{F_n^{(2)}\}$, which are calculated within the linear response, into this equation. The solution of the above equation is

$$
\begin{aligned}
\mathcal{E}_j(\omega_s)&=\mathcal{E}e^{iq_s j}+\overline{\mathcal{E}}e^{iq_s(N+1-j)}\\
&\quad-\sum_n\frac{\sin K_s j}{2\cos K_s-2\cos q_s}[\tilde{A}^{(1)}(K_n)+\tilde{A}^{(3)}(K_n)],
\end{aligned}
\tag{A21}
$$

where

$$
\tilde{A}^{(1)}(K_n)=B_s^{(1)}\left(\frac{2}{N+1}\right)^{1/2}\frac{F_n^{(3)}}{E_1(n)-\omega_s-i\Gamma}
\tag{A22}
$$

$$
\begin{aligned}
\tilde{A}^{(3)}(K_n)&=B_s^{(3)}\left(\frac{2}{N+1}\right)^{1/2}\\
&\quad\times\Bigg\{\sum_m A(K_n,K_m;\omega_1,\omega_2)F_n^{(2)}F_m^{(2)}F_m^{(1)*}\\
&\quad+\sum_m\sum_{n',m'} B(K_n,K_m,K_{n'},K_{m'};\omega_1,\omega_2)\\
&\quad\times F_{n'}^{(2)}F_{m'}^{(2)}F_m^{(1)*}\Bigg\}.
\end{aligned}
\tag{A23}
$$

In the same manner as for the linear response, we obtain the equation to determine $F_n^{(s)}$ as

$$
\begin{aligned}
&\left(\frac{N+1}{2}\right)^{1/2}\left[1+\frac{B_s^{(1)}}{2\cos K_n-2\cos q_s}\frac{1}{E_1(n)-\omega_s-i\Gamma}\right]F_n^{(s)}\\
&\quad+\left(\frac{N+1}{2}\right)\frac{\tilde{A}^{(3)}(K_n)}{2\cos K_n-2\cos q_s}\\
&\quad=\mathcal{E}\frac{\sin K_n}{2\cos K_n-2\cos q_s}[(-1)^n e^{iq_s(N+1)}-1]\\
&\qquad+\overline{\mathcal{E}}\frac{\sin K_n}{2\cos K_n-2\cos q_s}[(-1)^n-e^{iq_s(N+1)}].
\end{aligned}
\tag{A24}
$$

Assuming the outer signal fields from the front and back surfaces as

$$
\mathcal{E}_f e^{-ik_0 j}
\tag{A25}
$$

and

$$
\mathcal{E}_b e^{ik_0(j-N-1)},
\tag{A26}
$$

respectively, we obtain the Maxwell's boundary conditions at the front surface, as

$$
\mathcal{E}_f=\mathcal{E}+\overline{\mathcal{E}}e^{iq_s(N+1)},
\tag{A27}
$$

$$
\begin{aligned}
\mathcal{E}_f(e^{-ik_0}-1)&=\mathcal{E}(e^{iq_s}-1)+\overline{\mathcal{E}}(e^{-iq_s}-1)e^{iq_s(N+1)}\\
&\quad-\sum_n\frac{\sin K_n}{2\cos K_n-2\cos q_s}[\tilde{A}^{(1)}(K_n)\\
&\quad+\tilde{A}^{(3)}(K_n)],
\end{aligned}
\tag{A28}
$$

and at the back surface, as

$$
\mathcal{E}e^{iq_s(N+1)}+\overline{\mathcal{E}}=\mathcal{E}_b,
\tag{A29}
$$

$$
\begin{aligned}
&\mathcal{E}(1-e^{-iq_s})e^{iq_s(N+1)}+\overline{\mathcal{E}}(1-e^{iq_s})\\
&\quad-\sum_n\frac{(-1)^n\sin K_n}{2\cos K_n-2\cos q_s}[\tilde{A}^{(1)}(K_n)+\tilde{A}^{(3)}(K_n)]\\
&\quad=\mathcal{E}_b(1-e^{-ik_0}).
\end{aligned}
\tag{A30}
$$

Solving the simultaneous equations (A24),(A27),(A28), (A29),(A30), we can determine $\mathcal{E},\overline{\mathcal{E}},\mathcal{E}_f$, $\mathcal{E}_b$, and $F_n^{(s)}$.

[1] E. Hanamura, Solid State Commun. **62**, 465 (1987).
[2] E. Hanamura, Phys. Rev. B **37**, 1273 (1988).
[3] J. Yumoto, S. Fukushima, and K. Kubodera, Opt. Lett. **12**, 832 (1987).
[4] Y. Masumoto, M. Yamazaki, and H. Sugawara, Appl. Phys. Lett. **53**, 1527 (1988).
[5] T. Takagahara, Phys. Rev. B **39**, 10 206 (1989).
[6] L. Banyai, Y. Z. Hu, M. Lindberg, and S. W. Koch, Phys. Rev. B **38**, 8142 (1988).
[7] F. C. Spano and S. Mukamel, Phys. Rev. A **40**, 5783 (1989).
[8] T. Kataoka, T. Tokizaki, and A. Nakamura, Phys. Rev. B **48**, 2815 (1993).
[9] *Nonlinear Optical Materials*, edited by J. V. Moloney (Springer-Verlag, New York, 1998).
[10] T. Takagahara, Phys. Rev. B **36**, 9293 (1987).
[11] Y. Kayamuma, Phys. Rev. B **38**, 9797 (1988).
[12] Y. Ohfuti and K. Cho, Phys. Rev. B **51**, 14 379 (1995).
[13] K. Cho, H. Ishihara, and Y. Ohfuti, Solid State Commun. **87**, 1105 (1993).
[14] H. Ishihara and K. Cho, Phys. Rev. B **53**, 15 823 (1996).
[15] K. Cho, J. Phys. Soc. Jpn. **55**, 4113 (1986).
[16] H. Ishihara and K. Cho, Phys. Rev. B **48**, 7960 (1993).
[17] H. Wang, K. Ferrio, D. G. Steel, Y. Hu, R. Binder, and S. Koch, Phys. Rev. Lett. **71**, 1261 (1993).
[18] H. Ishihara and K. Cho (unpublished).
[19] H. Ishihara and K. Cho, Phys. Rev. B **42**, 1724 (1990).
[20] H. Ishihara and K. Cho, Int. J. Nonlinear Opt. Phys. **1**, 287 (1991).
[21] K. Cho and M. Kawata, J. Phys. Soc. Jpn. **54**, 4431 (1985).
[22] H. Ishihara (unpublished).
[23] E. L. Ivchenko, A. I. Nesvizhskii, and S. Jorda, Phys. Solid State **36**, 1156 (1994).
[24] M. Hübner, J. Kuhl, T. Stroucken, A. Knorr, S.W. Koch, R. Hey, and K. Ploog, Phys. Rev. Lett. **76**, 4199 (1996).
[25] S.S. Jha, J.R. Kirtley, and J.C. Tsang, Phys. Rev. B **22**, 3973 (1980).
[26] K. Akiyama, N. Tomita, Y. Nomura, and T. Isu, Appl. Phys. Lett. **75**, 475 (1999).
[27] H. Ishihara, K. Cho, K. Akiyama, N. Tomita, Y. Nomura, and T. Isu, Proceedings of the 25th International Conference on the Physics of Semiconductors [Springer Proc. Phys. **87**, 593 (2001).]
[28] K. Akiyama, N. Tomita, T. Nishimura, Y. Nomura, and T. Isu (unpublished).